



OPEN ACCESS

EDITED BY

DelWayne Roger Bohnenstiehl,
North Carolina State University,
United States

REVIEWED BY

Alexandre Schimel,
Geological Survey of Norway, Norway
Emma Cotter,
Pacific Northwest National Laboratory
(DOE), United States

*CORRESPONDENCE

Peter Feldens,
✉ peter.feldens@io-warnemuende.de

SPECIALTY SECTION

This article was submitted to Acoustic
Remote Sensing,
a section of the journal
Frontiers in Remote Sensing

RECEIVED 07 July 2022

ACCEPTED 10 February 2023

PUBLISHED 22 February 2023

CITATION

Feldens P, Held P, Otero-Ferrer F,
Bramanti L, Espino F and
Schneider von Deimling J (2023), Can
black coral forests be detected using
multibeam echosounder “multi-detect”
data?

Front. Remote Sens. 4:988366.
doi: 10.3389/frsen.2023.988366

COPYRIGHT

© 2023 Feldens, Held, Otero-Ferrer,
Bramanti, Espino and Schneider von
Deimling. This is an open-access article
distributed under the terms of the
[Creative Commons Attribution License
\(CC BY\)](https://creativecommons.org/licenses/by/4.0/). The use, distribution or
reproduction in other forums is
permitted, provided the original author(s)
and the copyright owner(s) are credited
and that the original publication in this
journal is cited, in accordance with
accepted academic practice. No use,
distribution or reproduction is permitted
which does not comply with these terms.

Can black coral forests be detected using multibeam echosounder “multi-detect” data?

Peter Feldens^{1*}, Philipp Held², Francisco Otero-Ferrer³,
Lorenzo Bramanti^{4,5}, Fernando Espino³ and
Jens Schneider von Deimling²

¹Leibniz Institute for Baltic Sea Research Warnemünde, Rostock, Germany, ²Marine Geophysics and Hydroacoustics, Institute of Geosciences, Kiel University, Kiel, Germany, ³Grupo en Biodiversidad y Conservación (IU-ECOQUA), Universidad de Las Palmas de Gran Canaria, Telde, Spain, ⁴CNRS, Laboratoire d’Ecogéochimie des Environnements Benthiques, LECOBS, Sorbonne Université, Paris, France, ⁵Under The Pole Expeditions, Concarneau, France

The black coral *Anthipatella wollastoni* forms marine animal forests in the mesophotic zone. The spatial extent of black coral forests is not well known in many regions. Due to its protein and chitin skeleton, the coral is difficult to image using acoustic remote sensing techniques compared to corals with carbonate skeletons. Several manufacturers have recently introduced an additional data type to their multibeam echosounders, called “multi-detection,” which provides additional target detections per beam in addition to the primary bottom detection. In this study, we used a Norbit chirp multibeam echosounder in multi-detect mode to acquire up to three targets in each beam in an area of black coral below 45 m depth off the coast of Lanzarote (Canary Islands, Spain). Multi-detect allows features above and below the primary bottom detection to be identified without the need to store and process water-column data. Black coral can be detected by comparing “multi-detection” data with ground truthing by technical divers and underwater cameras. However, the repeatability of the detections is limited and further sensitivity studies are required.

KEYWORDS

multibeam echo sounders, multi-detect, Lanzarote, *Anthipatella wollastoni*, marine animal forests, habitat mapping

1 Introduction

Marine animal forests (MAFs) are composed of sessile, suspension-feeding organisms that form complex 3D hotspots of marine biodiversity (Rossi et al., 2021). Information on the ecosystem function and distribution of MAFs is lacking, particularly in mesophotic water depths (30 m–200 m), which are beyond the reach of satellite remote sensing. In order to effectively map and protect habitats at these depths, studies of the biodiversity, ecosystem functioning and spatial extent of MAFs are required. Diving and point sampling are commonly used to study these keystone ecosystems. Detecting MAFs and mapping their extent using acoustic remote sensing would provide spatial information at scales from metres to kilometres, complementing point based and high resolution photogrammetric techniques. The need for information at such scales to manage, conserve and understand the ecology of the seascape has recently been highlighted (Rossi et al., 2021).

The detection of benthic habitats in acoustic data can range from straightforward to challenging. Benthic life can be observed by acoustic remote sensing both below the seafloor

[e.g., changes in physical sediment structure by seagrass rhizomes, endobenthic life (Schulze et al., 2021)] and above the seafloor (e.g., MAFs, macrophytes and macroalgae). Bathymetric grids, backscatter imagery and derived data thereof have been used for modern habitat mapping with excellent results for many types of seafloor (Blondel and Gómez Sichi, 2009; Brown et al., 2011; Che Hasan et al., 2012; Parnum and Gavrilov, 2012). These approaches have allowed the mapping of deep benthic habitats of cold water corals with calcium carbonate skeletons such as *Lophelia Pertusa* (Roberts et al., 2005; Glogowski et al., 2015; Lim et al., 2020), benthic habitats dominated by mussel beds (Snellen et al., 2008) or polychaetes such as *Lanice conchilega* (Heinrich et al., 2017), which influence seafloor roughness and backscatter intensity. Multibeam echosounder (MBES) derived point clouds were used to detect seagrass meadows (Held and Schneider von Deimling, 2019). Macroalgae, including kelp forests, that extend sufficiently high into the water column for their echoes to occur above the seafloor echo were detected by single beam echosounders (Minami et al., 2014), MBES bathymetry and backscatter data (McGonigle et al., 2011) and water column data (Schimel et al., 2020; Porskamp et al., 2022).

Water column data are used for a variety of purposes, including navigational purposes, such as detecting shipwrecks at shallow depths (Wyllie et al., 2015), tracking zooplankton migration and gas release from the seafloor (Schneider von Deimling and Weinrebe, 2014; Weinrebe, 2020), detecting kelp forests (Colbo et al., 2014), or oceanographic purposes, such as imaging internal waves (Colbo et al., 2014). It is expected that water column data will also be suitable for detecting MAFs such as black coral forests. Water column data require the storage of full-beam time series. However, the storage of water column data results in data acquisition rates of up to 70 MB/s (for an R2Sonic 2024 system). Therefore, MBES water column data have only recently been incorporated into habitat mapping approaches (Porskamp et al., 2022) due to the volume of data, the difficulty of processing and interpretation, and the lack of suitable software.

Norbit recently designed the so-called “Multi-Detect Algorithm,” which consists in detecting up to three targets per beam during data acquisition. This constitutes a favourably lightweight alternative compared to the traditional water column data, which store the entire beam time-series. Other manufacturers implement similar data types, with possibly different algorithms and terminology (e.g., Kongsberg’s “extra detections,” ELAC and RESON’s “quality flags”). A general description of the method can be found in (Christoffersen, 2013). Before depth is output from an MBES, such systems analyse the beam formed echo time series data using bottom detection algorithms, which is key to obtaining the final bathymetry. MBES are characterised by sophisticated bottom detection algorithms that decide on the fly where the bottom should be in such time series data. Modern MBES use two bottom detection algorithms, based on detection of amplitude peaks or zero phase crossings by a split array (Lurton et al., 2015). Consequently, depth data derived from MBES can be thought of less as a direct measurement and more as a product of the system’s bottom detection algorithms. This algorithmic decision is often uncertain, especially in complex seafloor environments. For this reason, MBES systems allow the storage of less likely alternative solutions that are output by the bottom detection algorithm in addition to the primary seafloor echo detection, technically referred to as “multi-detect” soundings or “extra detections”. The data used in this study were acquired with a prototype NORBIT firmware, which for our system

allows the recording of multi-detect data with up to three bottom detection solutions (e.g., for better imaging of ship wrecks) in each beam, based on proprietary sensitivity thresholds implemented in the bottom detection algorithm.

The potential of these “multi-detect data” (hereafter MD) to improve habitat mapping by measuring both the actual seafloor and the top of the canopy—with an example of kelp forests—has been recognised (Christoffersen, 2013). To our knowledge, no studies have used multi-detect data for actual habitat mapping, although Schneider von Deimling et al. (2007) used it for gas flaring detection. Hamana and Komatsu (2021) and Held and Schneider von Deimling (2019) used misclassifications of the bottom detection algorithm to identify benthic habitats in point cloud data (brown algae and seagrass, respectively). The target habitat of this study, the black coral forests formed by *Anthipatella wollastoni* (Gray, 1857) off the coast of Lanzarote, Spain, appears geometrically similar to a vegetated seabed, with corals protruding from the seabed a few decimetres into the water column (Figure 1). However, they are difficult to identify acoustically in traditional morphological and backscatter maps based on acoustic remote sensing data due to the coral’s chitin and protein skeleton and its appearance on rough seafloor outcrops with steep slopes (Czechowska et al., 2020).

In this study, we investigate whether the output of Norbit’s multi-detect algorithm can be used to detect black coral forests composed of *Anthipatella wollastoni*. This keystone MAF, together with other black coral species, is the result of centuries or millennia of biological activity (Roark et al., 2006; Rossi et al., 2017) and may dominate circalitoral depths (ca. 50–200 m) due to environmental factors that favour their settlement and growth (de Matos et al., 2014; Rossi et al., 2017), although information on their extent at these depths is currently limited.

2 Materials and methods

2.1 Multibeam echosounder survey

A MBES survey was carried out off the coast of Lanzarote, Spain (Figures 2A, B) from 21 to 25 October 2021 using an integrated NORBIT iWBMS MBES together with an Applanix Wavemaster inertial navigation unit. The MBES was mounted on the port side of a 12 m long fibreglass boat using a custom made metal bracket. Our measurements involved real-time kinematics (RTK), supported by a Global Navigation Satellite System (GNSS) reference station operated by GRAFCAN in the municipality of TÍAS, just 2.6 nm from the survey area. The resulting accuracy in position and height was between 2 cm and 5 cm. The echosounder was operated at 400 kHz in chirp mode with a bandwidth of 80 kHz, giving a theoretical range resolution of 9 mm. The survey speed was approximately 4 knots. We covered the survey area several times with different MBES acquisition modes, focusing on coverage between 40 m and 110 m water depth. We first concentrated on acquiring bathymetric data, then sailed the lines to collect multi-frequency information (not discussed in this study) and finally recorded MD in a third run. For MD recording, the swath angular opening was set to 100°, split into 512 beams. Sound velocity was measured on-line with an AML keel probe and intermittently

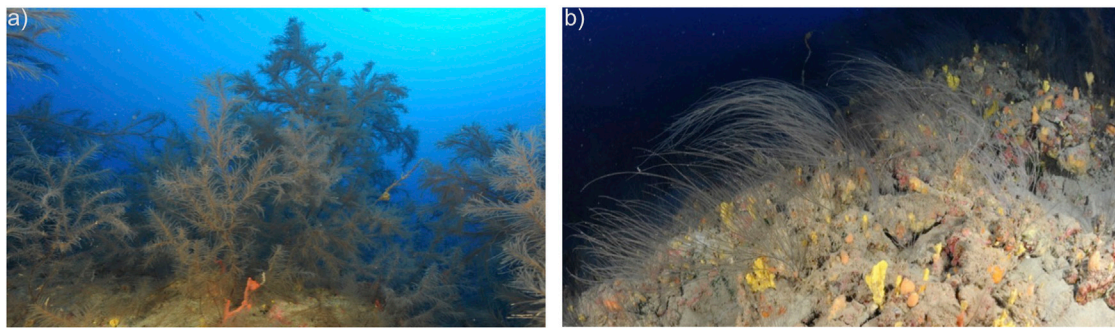


FIGURE 1
(A) *Antipathella wollastoni* forms dense forests. (B) It is replaced by *Antipathes furcata* at around 80 m water depth in the investigation site.

with a vertical cast and was found to be constant throughout the survey period, ranging from 1,531.4–1,531.8 m/s.

2.2 Bathymetric data pre-processing

MBES, motion sensor and sound velocity data were loaded into QPS Qimera 2.4. Binary inertial measurement unit (IMU) data recorded with the Applanix Wavemaster were reloaded to apply true heave calculation, which is only available in post-processed data. We then ray traced the soundings, with a sound velocity profile that was almost constant with depth, and roll calibrated our system using Qimera 2.4. Our ellipsoidal height measurements from the RTK antenna had occasional drop-outs of a few minutes, which we interpolated in Qimera. Therefore, tidal reduction was successfully achieved by vertical referencing to mean sea level using the 2008 Earth Gravity Model (Pavlis et al., 2012), and lines recorded on different days and tidal phases matched. Spurious echoes were then manually removed by human experts inspecting the data in 2D and 3D editors. The final grids presented were generated using a spline with tension gridding and an interpolation algorithm.

2.3 Processing of multidetected data

With our prototype NORBIT iWBMS firmware, we acquired MD in the hope of detecting black corals extending into the water column. In the field, we set the sensitivity slider controlling the proprietary Norbit algorithm to report MD at a location known for black coral occurrence (Ridge A, Figure 2B) and kept the setting constant for the following survey. The data were stored in the Seabat 7k (s7k) data format developed by Reson A/S. Unfortunately, it was confirmed by the manufacturer that the beta firmware reported incorrect intensity values for MD. The intensity values were not used in this study. The survey produced 27,898,462 soundings, which included 601,846 MD (2.2%, raw MD shown in Figure 2C).

The MD were filtered to account for systematic and environmental misclassifications and artefacts. An example of the processing workflow is shown in Figure 3. In particular, there were many artefacts in areas deeper than 80 m in the SW part of the study site, where MD appeared

related to the ship's roll movement during acquisition. These artefacts can be recognised visually as they form horizontal stripes across a ping or form extended dense blankets (Figure 3B) that are not recognised in overlapping survey lines. These artefacts and erroneous detections that were observed in the outer beams of some lines on sandy seabeds (Figure 3B) were removed manually on a line-by-line basis before data analysis. The manual data cleaning is similar to the well-established manual cleaning of bathymetric data, but clearly adds subjectivity to our analysis. Following this manual filtering, 320,077 MD remained.

After the manual editing, filters were applied. We focused on depths between 40 m and 110 m and therefore filtered out MD shallower than 40 m and deeper than 110 m. The deeper value corresponds to the maximum depth our portable MBES could measure in the steep environment. MD can occur throughout the water column, e.g., due to the presence of fish or bubbles, or due to acquisition noise. We removed isolated MD, defined as three or fewer in $4\text{ m} \times 4\text{ m}$ cells. The number of MD in each cell varied from 1 to 581. Our third filter was to remove MD located at a vertical distance of more than 2.5 m from the bathymetric surface. This value was defined manually, accounting for the occasionally rough seafloor and the uncertainty of the bathymetric surface. The vertical distance of MD to the seafloor is their depth difference to a bathymetric surface, which was calculated without including any MD. The volcanic seafloor is rough and the uncertainty of the bathymetric surface at a 95% confidence level can exceed several metres, especially in areas with steeper morphology (Supplementary Figure S1). Accepting MD below the bathymetric surface is necessary because the top of the coral canopy may be registered as the primary bottom detection point for dense coral fields. We found that false positive MD were very common in very steep and complex seafloor morphologies, probably due to multipath reflections. We therefore removed all MD where the slope was greater than 40° . This affected 4.0% of the area. Following this automatic filtering, 113,802 MD remained.

To analyse the spatial distribution of MD relative to the ground truth data, the filtered MD were further processed into three gridded variables of $4\text{ m} \times 4\text{ m}$ cell size (i.e., twice the resolution of the underlying bathymetric grid). The calculations were carried out in QGIS version 3.22. The first gridded variable (MD_{USL}) is the number of unique survey lines contributing at least one MD to a cell. In addition to survey parameters such as ship speed, the number of MD in a cell is controlled by the number of survey lines covering it. This

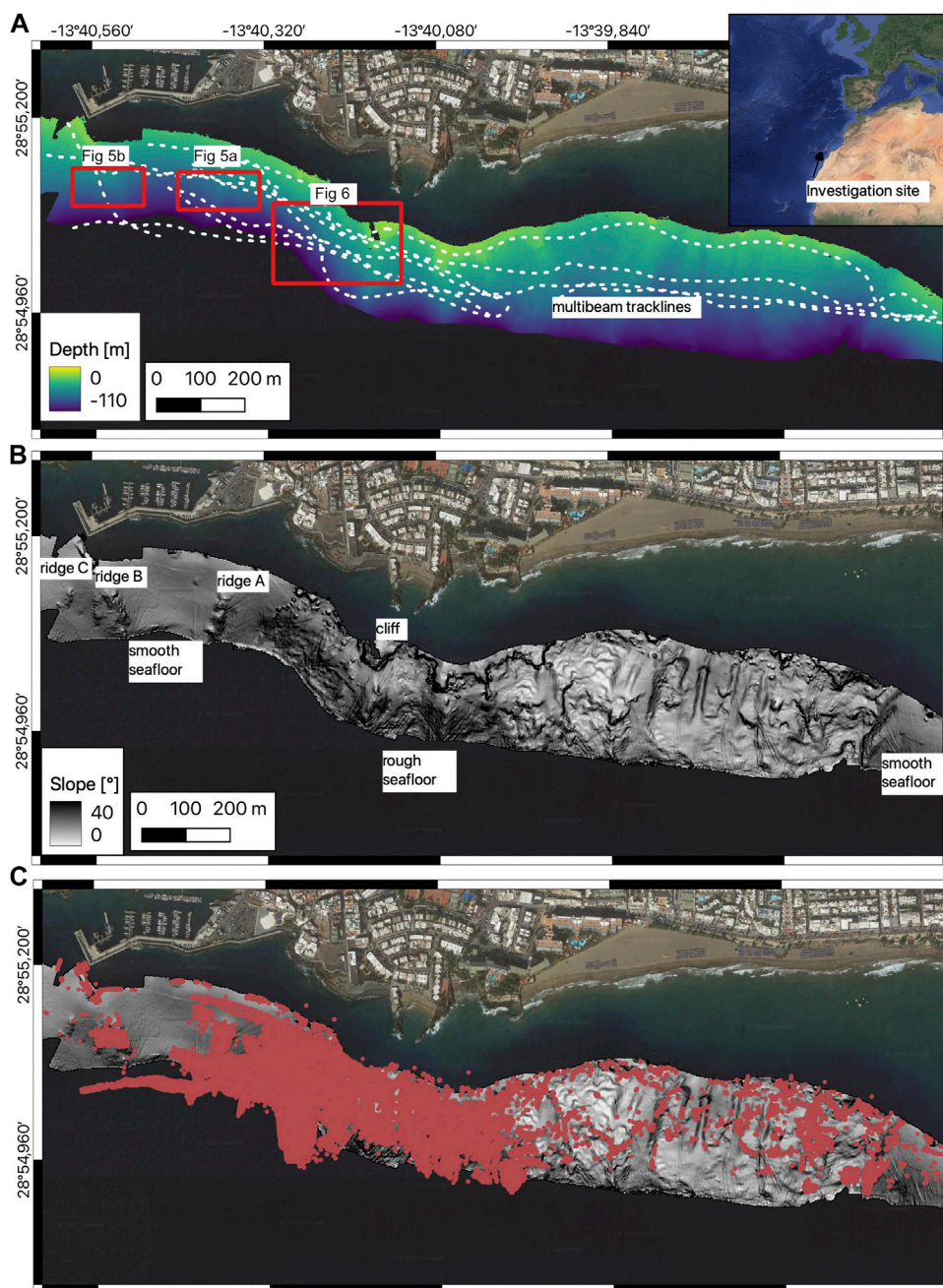


FIGURE 2
 (A) Bathymetric map of the investigation site. Dashed white lines show tracklines acquired for survey with the MD algorithm. (B) Slope map of the investigation site. The location of a steep cliff, and the ridges A, B and C are indicated. (C) Plot of raw MD.

variable takes values between 0 and 7 across the site (Figure 3D). The second grid variable (MD_f) is MD_{USL} divided by the number of overlapping lines (Figure 3E). This variable takes values between 0 and 1 throughout the site. The third grid variable (MD_c) is the total number of MD per cell divided by the number of overlapping lines (Figure 3F). This variable takes values between 0 and 194 across the site. The motivation for creating these multiple gridded variables is that the number of overlapping lines is not constant across the study site and is therefore a confounding factor in the analysis of the spatial distribution of MD, and the line-by-line manual editing

process is unlikely to remove all MD artefacts. For example, a low MD_{USL} value of 1 and a low MD_f value (on a site where many lines overlap) would indicate a high confidence that these MD are false positives. For false positives related to acoustic noise due to roll movements, high values of MD_c are observed in addition, as all beams are affected. We consider MD_f values below 0.25 as false positives caused by remaining acoustic noise. The same value for MD_{USL} on another site covered by only one or a few lines (resulting in a higher value for MD_f) would only indicate a lack of sufficient overlap to arrive at a firm conclusion.

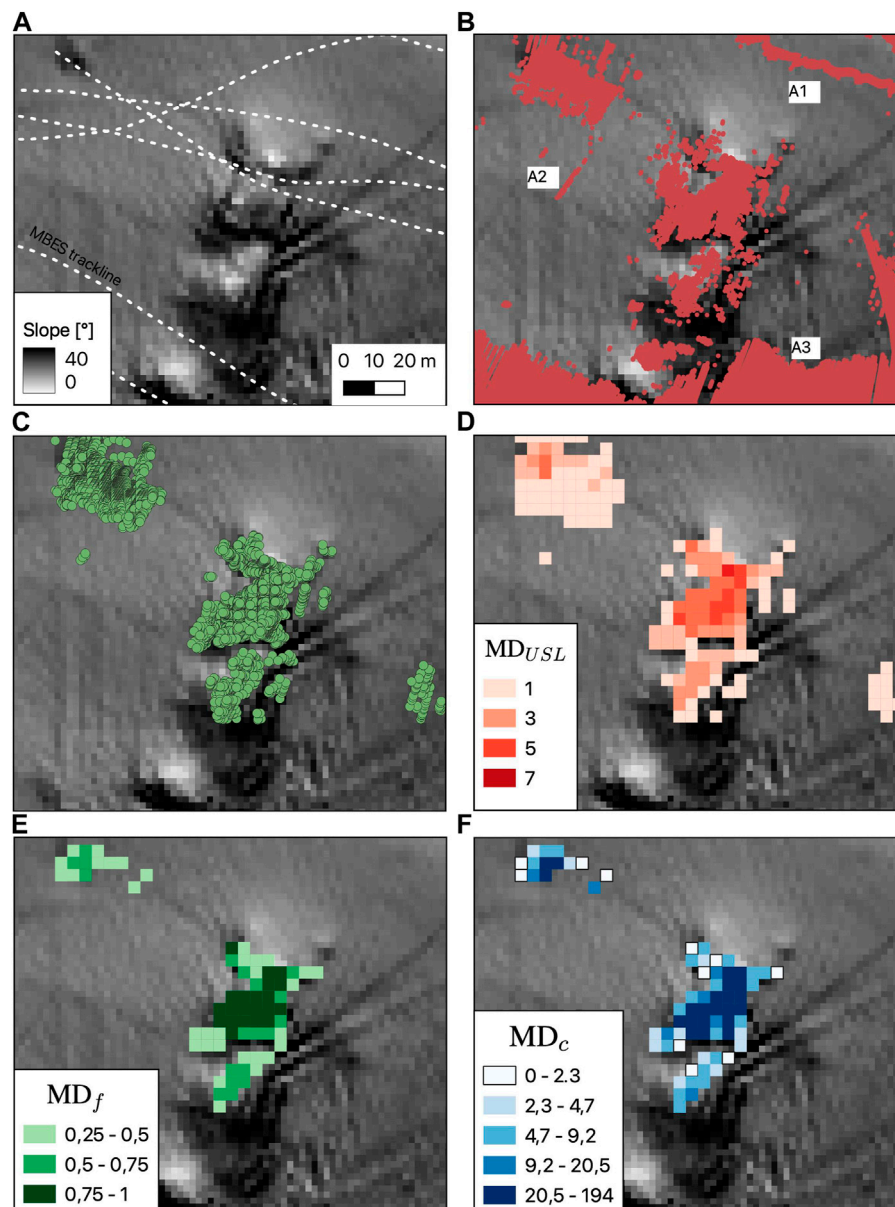


FIGURE 3

(A) MBES track lines crossing Ridge A (refer to Figure 2 for location). A slope map is displayed in the background. (B) Raw MD. Artifacts include elongated lines of MD on sandy seafloor on the outer beams (A1), short rails of MD on a single ping (A2) and extended blankets of MD in deeper waters associated with roll movements during the survey (A3). (C) Filtered MD. MD in the south of the ridge were filtered due to excessive elevation above the seafloor. (D) MD_{USL} (E) MD_f. (F) MD_c.

2.4 Ground truthing

The ground-truth dataset is composed of underwater video footage acquired on 6 sites: 3 sites by divers and 3 sites by drop-camera. Technical divers provided descriptions, photos and underwater video footage taken with a GoPro Hero 9 camera. To accurately locate the dive sites, technical divers with rebreathers left an Ultra Short Baseline (USBL) modem on the seafloor, which could be located to within a few metres from the survey vessel. Technical diving does not produce bubbles during the dive, which could interfere with the acoustic measurements.

In addition to the video recorded by the divers, underwater photos were taken every second from the survey vessel at three sites by attaching a GoPro video camera (GoPro Hero 7) to a rope with extra weight at the end. The rope was lowered to the seabed (indicated by the decreasing tension of the rope). As the boat drifted at approximately 1 kn, continuous video was recorded. The position of the boat was used as a co-ordinate reference for the GoPro images. However, this was subject to uncertainty due to the presence of local currents and the fact that the boat was constantly moving while the weight of the camera was touching the seabed. Therefore, photos were selected where the camera

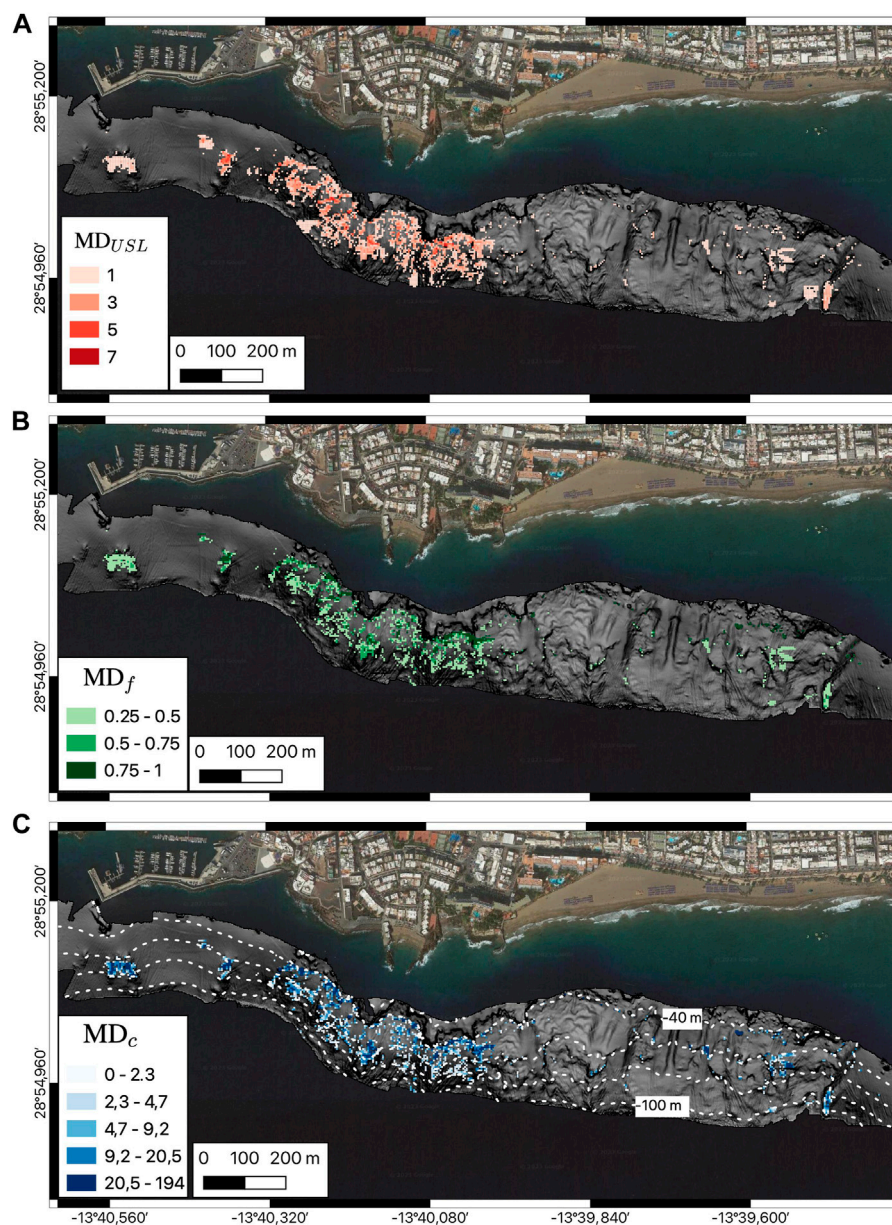


FIGURE 4

(A) Grid of MD_{USL} . (B) Grid of MD_f . (C) Grid of MD_c . Isobaths are displayed as white dashed lines.

initially touched the seabed, but some deviation from the boat's position may remain. Photos were manually classified as 1) no black coral present and 2) black coral present.

3 Results

3.1 Morphology and geology

The study area ranges from a minimum of 20 m to a maximum of 110 m water depth and is located south of the island of Lanzarote. The morphology is shown in Figure 2A. Due to the volcanic origin of the islands, the slopes are steep and the

water depth reaches 100 m at a distance of about 350 m (western part) to 550 m (eastern part) from the coast. A striking feature is an almost vertical cliff in the centre of the survey area, where the seabed drops rapidly from 20 m to 45 m. Large parts of the survey area are covered by sand, but basaltic outcrops are frequent and result in a rough seabed morphology, especially in the central and eastern part of the survey area, which is reflected in the displays of seabed slope (Figure 2B). The mean slope value of the survey area is 21.6° , with the highest values in the central part and the lowest values in the eastern part of the area. Towards the west, isolated ridges raised from the surrounding sandy seabed allow for easier ground-truthing of acoustic data with underwater video cameras, while diving

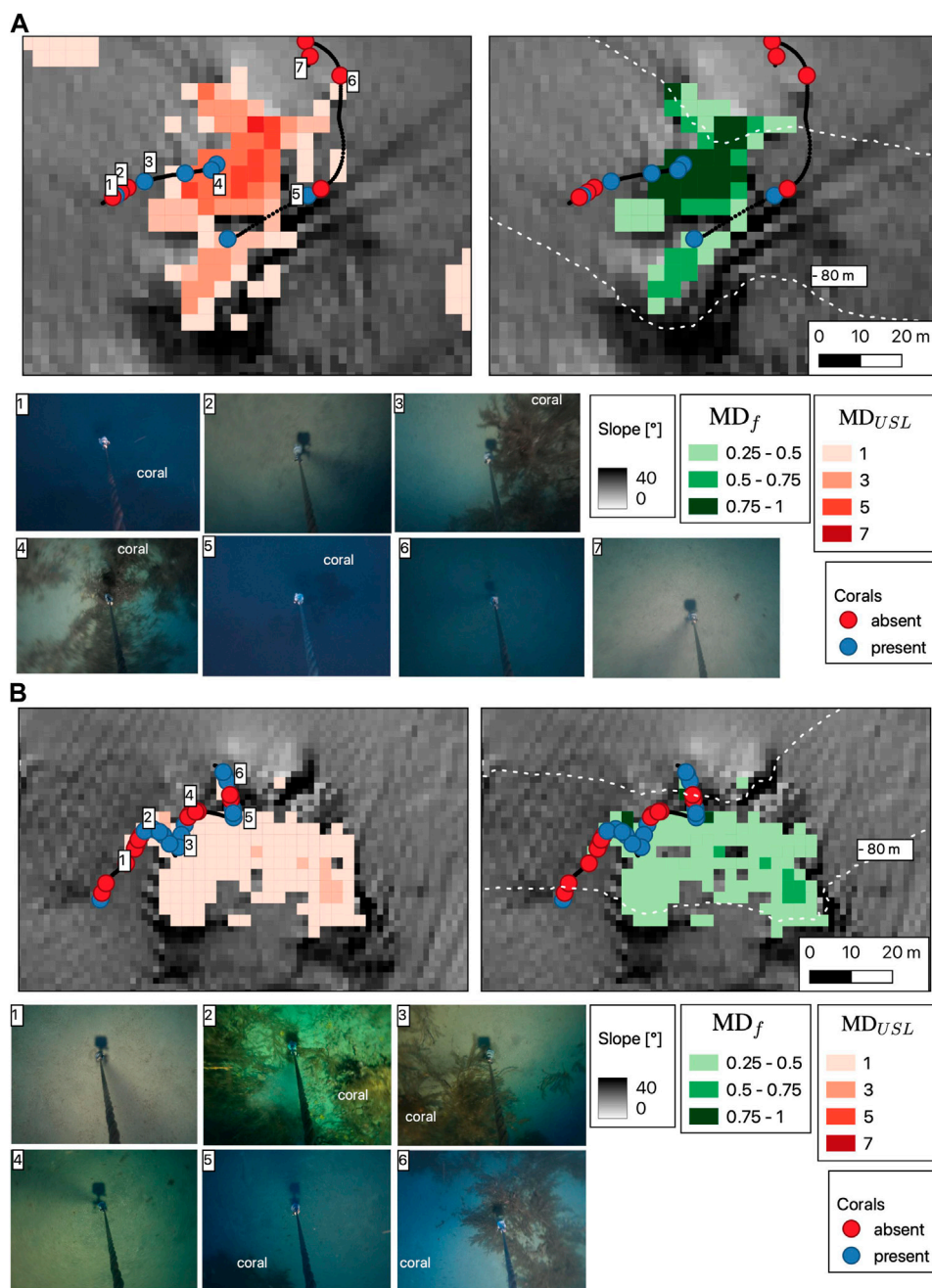


FIGURE 5
 Comparison of ground truthing information with the grids of MD_{USL} and MD_f . (A) Ridge A. (B) Ridge B. Refer to Figure 2 for location.

operations focused on the morphologically more complex central part of the survey area.

3.2 Multidetect soundings

3.2.1 Spatial distribution

Unfiltered MD (Figure 2C) are mostly concentrated over the central survey area, while less MD are observed in the east (with reduced survey line coverage, Figure 2A) and on the sandy seabed in

the west. After filtering, this trend is maintained, with the highest values of MD_c in the central survey area (Figure 4C). The highest values of MD_f and MD_{USL} in the central part of the survey area are below the steep cliff on the rough seabed (Figures 4A, B). Few MD are located below 80 m depth, with values of 1–2 for MD_{USL} and less than 0.25 for MD_f . Towards the west, on the smooth seafloor, MD are present in only a few grid cells. However, two fields of MD are located on two ridges A and B (marked in Figure 2B). A third ridge C (marked in Figure 2B) in the far west of the survey area shows no MD. From the central survey area towards the east, the value of MD_c

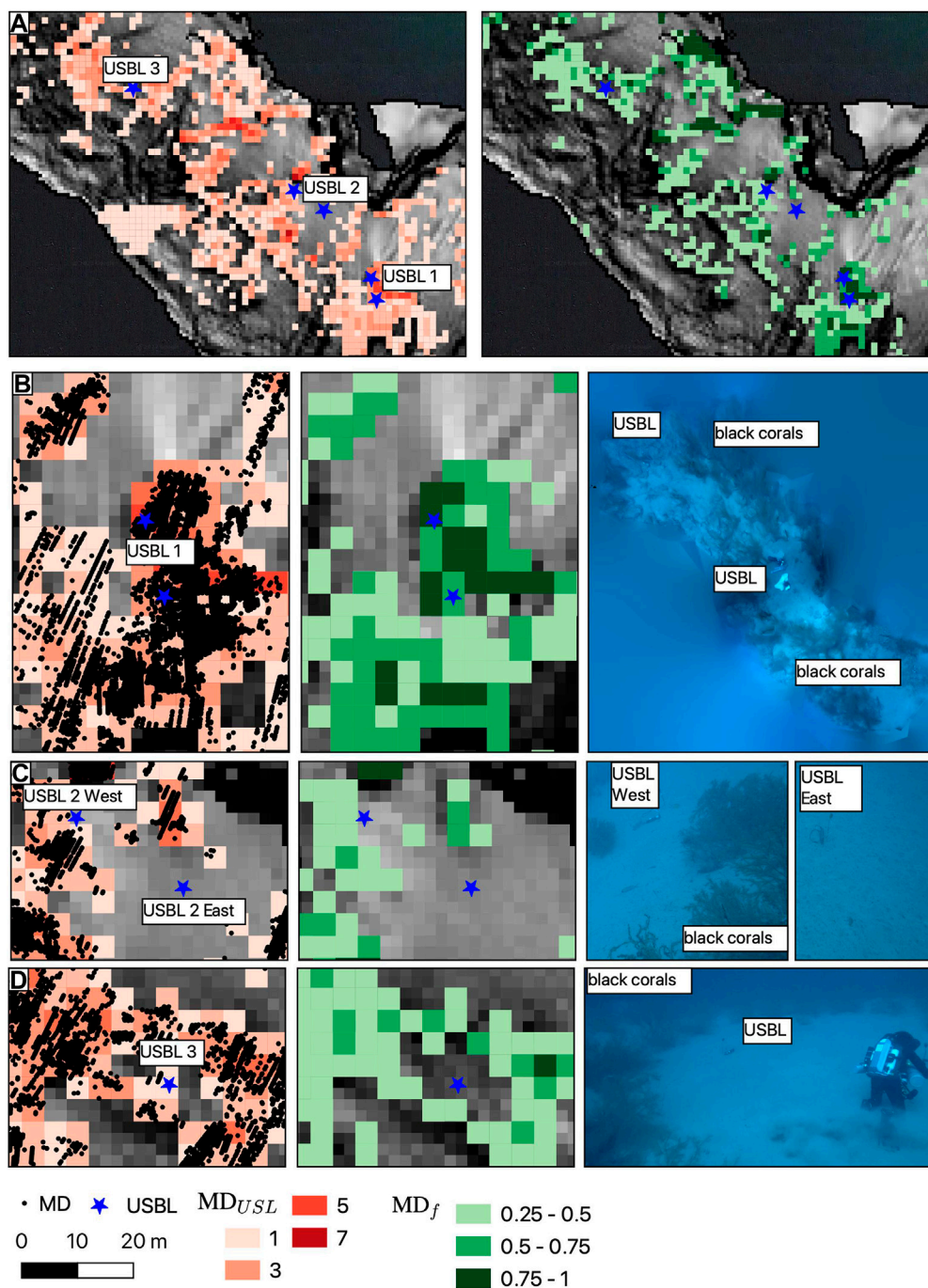


FIGURE 6 Grid of MD_{USL} and MD_f (A) for the location with diver ground truthing, showing black coral occurrence at USBL sites 1 (B), 2 (C) and 3 (D). For USBL site 1, a photo mosaic was created from a diver-recorded video.

decreases significantly (Figure 4C), and MD generally form smaller fields. Some MD appear close to the eastern boundary of the survey area and disappear on the smooth seabed.

The MD characteristics on ridges A and B are shown in detail in Figure 5. On ridge A, MD are reported on the top and flanks (except the southern flank) of the ridge and are generally imaged on multiple survey lines, indicated by high MD_{USL} values. On this site, MD are found down to 80 m water depth. On ridge B, MD

cover the eastern and western flank and parts of the ridge plateau. Here, MD are found down to 83 m water depth. The ridge continues at greater depths, but the deeper plateau and southern flank are not covered by MD. It is noteworthy that the majority of MD on ridge B are only recorded on a single survey line (MD_{USL} value of 1) and are not repeated on additional survey lines (MD_f generally less than 0.5, and less than 0.25 and thus interpreted as false positives for some grid cells).

3.2.2 Ground truthing

Ground truthing by technical divers identified *Antipathella wollastoni* between 45 m and 80 m throughout the investigation site. Other black coral species (e.g., *Antipathes furcata*, Gray, 1857) are gradually replacing *Antipathella wollastoni* communities below 80 m (Figure 1).

Figure 5 shows the distribution of MD and the observation of sand and corals in the underwater video camera images at ridges A and B. On the western flank of the ridge A site (Figure 5A), the underwater video footage confirms the presence of black corals in the area with MD. However, the boundaries between MD and the video footage do not coincide. The black coral observed in the video footage extends 5–10 m from the area of MD. A possible black coral just west of ridge A, difficult to see in the underwater video, does not correlate with MD.

For ridge B (Figure 5B), the presence of corals determined by ground truthing is generally consistent with the location of MD. To the north, there is an offset of approximately 2 m (which is expected to be well within the positional uncertainty) between the onset of MD and the presence of corals in the underwater video footage. An isolated image with corals is located outside the area of MD to the west.

Underwater videos taken by technical divers can be compared with MD for sites where a USBL could be placed on the seabed. An overview of USBL positions in the morphologically complex central part of the survey area is shown in Figure 6. At Site 1, two USBLs were positioned on a ridge, one on the northern tip, the other on the southern tip of the ridge. The northern one was positioned at 47.8 m depth, the southern one at 47.6 m depth. The ridge is covered with dense patches of black coral. The majority of survey lines (MD_f greater than 0.5) report MD at this location. At site 2, the USBLs were positioned on sand approximately 20 m apart along a NW-SE line. The northwestern USBL was at a depth of 53 m, the southeastern at 52 m. The south-eastern USBL is on sand, while the northwestern USBL is in an area of increased patchy coral cover. MD reflect this pattern and are absent in the SE, while MD are observed on some lines (MD_f less than 0.5) in the NW. At site 3 a USBL was positioned on a round sand clearing surrounded by black coral. The circle was approximately 5 m in diameter according to the divers. This setting agrees with the absence of MD around the USBL positions, although the distance from the USBL position to the onset of MD exceeds the 5 m observed by divers, and MD are not observed in every line in this location (MD_f between 0.25 and 0.75).

4 Discussion

Our study demonstrates both the possibilities and problems of using MD for habitat mapping. The sequence of absent/present MD when crossing the location of *A. wollastoni* in underwater images (Figure 5) confirms a relationship with black coral occurrence, although a positional uncertainty of the ground truthing by camera exists due to currents and boat movements. Similarly, photos of black coral distribution by divers at the USBL locations (Figure 6) are consistent with the filtered MD pattern.

The presence of raw MD (Figure 2C) is, however, not indicative of the presence of black coral. MD artefacts occur in large numbers under low signal-to-noise survey conditions, for example, under strong roll motion, and require intense manual data cleaning. MD are also common in seafloor with steep morphology due to multipath effects. Multipath acoustic propagation, in turn, can occur not only on natural morphological structures, but also on man-made structures such as shipwrecks (Wyllie et al., 2015). Fish and bubbles in the water column also cause MD in MBES data (Schneider von Deimling et al., 2007). Filtering is required to remove MD not associated with black corals, and high values of MD_f are required to distinguish real targets from acoustic noise. Our filter thresholds exceed the biological background information on black corals in terms of depth range, height, and preferred slope (Czechowska et al., 2020). While *Antipathella wollastoni* normally occurs between 50 m and 200 m (de Matos et al., 2014; Rossi et al., 2017), it is locally replaced by *A. furcata* at 80 m depth. The average local coral height was measured to be $1.15 \text{ m} \pm 0.08 \text{ m}$ (Czechowska et al., 2020). Previous studies have also shown that the vast majority of corals occur on slopes below 40° (Czechowska et al., 2020).

Assuming that the majority of artefacts and water column targets such as fish have been removed by the manual and automatic filtering procedures, a remaining problem is the differentiation of MD caused by black corals and multipath effects. We made mixed observations on the link between MD distribution and rough seabed morphology, and there is evidence for both causes in our data set. The majority of MD are located above 80 m water depth (Figures 4C, 5). MD below 80 m are generally not repeated on other lines (Figure 4A), indicated by low MD_f and MD_{USL} values. This is consistent with a gradual replacement in coral species of *A. wollastoni* to *A. furcata* below 80 m water depth. The delicate shapes of *A. furcata* [ca. 20 cm high; Brito and Ocaña (2004)] are not expected to leave a trace in the acoustic data (Figure 1B). According to the map of slope (Figure 2B), it appears that depths below 80 m are just as commonly rough as above 80 m, while black corals occurrence ceases. Rough morphological features situated below 80 m water depth such as the southern flank of ridge B (Figure 5), ridge C (Figure 2B) or south of the USBL site 3 (Figure 6) do not cause MD. The reduced occurrence of MD below 80 m water depth, the limit of *A. wollastoni* occurrence, seems therefore unlikely to be related to morphological effects (it could be related to the effects of increasing acoustic footprint). However, there are MD in the vicinity of the vertical cliff in the central study area. Here, it can be assumed that MD form due to multipath reflection similar to harbour quay walls (Christoffersen, 2013). A number of MD were found in the unfiltered raw data at this site (Figure 2C). By setting a slope filter to 40° , we reduced the number of reported MD. However, several lines have MD adjacent to the cliff (north of USBL 2, Figure 6) and reports from divers passing along the cliff to the deeper coral sites (these reports could not be geo-referenced) indicate that these MD are false positives with regard to black coral presence. In contrast to false positives below 80 m water depth that are caused by acoustic noise, the multipath reflections are very repeatable with values for MD_f exceeding 0.75. Potentially, the backscatter intensity of multi-detect soundings can be used to further discriminate between MD caused by black coral and multipath reflections. The black corals are expected to have low backscatter intensities due to their chitin and protein skeletons (Goldberg et al., 1994). Unfortunately, our beta firmware did not correctly register MD intensities, so we could not explore this topic further in this study. However, when software allows

recording MD intensities, the relation of this intensity with the type of detected features should be part of future investigations.

A further problem with the use of MD in habitat mapping is the poor repeatability of black coral detections that are confirmed by ground truthing: Out of three lines on ridge B, black coral was mostly found to be present in one line and absent in the others (Figure 5B). In contrast, apparently isolated coral patches observed in underwater images did not cause MD. At ridge A, MD_f exceeded 0.75, and the values of MD_c are among the highest of the study site (Figures 4B, C). However, this observation is biased because this site was used to calibrate the initial MD algorithm sensitivity setting. The poor repeatability at other sites could be related to 1) the reference site having different physical parameters in terms of coral abundance/height and/or seafloor roughness causing multipath effects, and 2) an effect of acoustic incidence angle on MD recording (ridges A and B are covered by different angles of incidence as apparent from multibeam echo sounder tracklines; Figure 2A). The denser survey line spacing in the central survey site results in higher values of MD_c compared to the eastern survey site (Figure 4C). It is possible that fewer black coral forests exist in the eastern survey site. The seafloor complexity changes towards the east (Figure 2B) and fewer corals were observed here (Czechowska et al., 2020) based on limited ground truthing. However, it is more likely our survey missed many black coral forests entirely due to the lower survey line density. Future studies to understand and improve the sensitivity of multi-detection algorithms to black coral forests of varying coral abundance, height, as well as acoustic frequency and incidence angle, will be necessary to enable reliable mapping of the spatial extent of black coral forests.

Finally, a problem that prevents repeatable sensitivity studies is the proprietary nature of the multi-detection algorithms of the manufacturers. Details on the algorithms implemented by the different manufacturers would be necessary to allow the interpretation and comparison of results.

In conclusion, MD are a promising additional source of seafloor information that can be obtained from MBES surveys. The results show that *Antipathella wollastoni* off the coast of Lanzarote can be detected in MD acquired with a NORBIT MBES. Combined with ground truthing, MD may serve as a basis for improving distribution maps of black coral forests in the future. Despite the lack of studies, MD are also expected to be caused by a range of habitats. They may be useful for mapping other corals, seagrass [as suggested by point cloud analysis by Held and Schneider von Deimling (2019)], kelp forests [as suggested by Christoffersen (2013)] or other keystone MAFs.

Data availability statement

The datasets presented in this study can be found in online repositories. The names of the repository/repositories and accession number(s) can be found below: <https://doi.org/10.5281/zenodo.6786351>.

Author contributions

PF and FO-F conceived the study. FO-F leads the B-Charmed project. PF, PH, and JS did the acoustic survey, data processing and data interpretation. FO-F, LB, and FE did the ground truthing by technical diving. PF and JS wrote the original draft. PH, FO-F, LB, and FE edited the draft.

Funding

This study has been produced with the financial support from the LIFE Programme of the European Union, the French Office for Biodiversity (OFB) and the French Development Agency (AFD) through the LIFE4BEST Program. The contents of this document are the sole responsibility of the B-CHARMED (The Black Coral forests as unexplored Biodiversity Hotspots in the MAcaronesian Region: ecosystem functions and sErVICES analysed) project and can under no circumstances be regarded as reflecting the position of the European Union nor of the OFB and AFD.

Acknowledgments

We acknowledge Booking Dive Lanzarote SCP (especially Sonia and Nando) for its technical assistance with boat support during habitat mapping campaign. We greatly acknowledge the support by NORBIT and Pawel Pocwiardowski supplying us with prototype firmware and support. We would like to thank the reviewers for their detailed and thoughtful comments that have significantly improved the manuscript.

Conflict of interest

The authors declare that the research was conducted in the absence of any commercial or financial relationships that could be construed as a potential conflict of interest.

Publisher's note

All claims expressed in this article are solely those of the authors and do not necessarily represent those of their affiliated organizations, or those of the publisher, the editors and the reviewers. Any product that may be evaluated in this article, or claim that may be made by its manufacturer, is not guaranteed or endorsed by the publisher.

Supplementary material

The Supplementary Material for this article can be found online at: <https://www.frontiersin.org/articles/10.3389/frsen.2023.988366/full#supplementary-material>

References

- Blondel, P., and Gómez Sichi, O. (2009). Textural analyses of multibeam sonar imagery from stanton banks, northern Ireland continental shelf. *Appl. Acoust.* 70, 1288–1297. doi:10.1016/j.apacoust.2008.07.015
- Brito, A., and Ocaña, B. (2004). *Corales de las islas canarias: Antozoos con esqueleto de los fondos litorales y profundos*. La Laguna, Spain: Francisco Lemus, 477.
- Brown, C. J., Smith, S. J., Lawton, P., and Anderson, J. T. (2011). Benthic habitat mapping: A review of progress towards improved understanding of the spatial ecology of the seafloor using acoustic techniques. *Estuar. Coast. Shelf Sci.* 92, 502–520. doi:10.1016/j.ecss.2011.02.007
- Che Hasan, R., Ierodiaconou, D., and Laurenson, L. (2012). Combining angular response classification and backscatter imagery segmentation for benthic biological habitat mapping. *Estuar. Coast. Shelf Sci.* 97, 1–9. doi:10.1016/j.ecss.2011.10.004
- Christoffersen, J. T. (2013). “Multi-detect algorithm for multibeam sonar data,” in 2013 OCEANS-San Diego. 1–4.
- Colbo, K., Ross, T., Brown, C., and Weber, T. (2014). A review of oceanographic applications of water column data from multibeam echosounders. *Estuar. Coast. Shelf Sci.* 145, 41–56. doi:10.1016/j.ecss.2014.04.002
- Czechowska, K., Feldens, P., Tuya, F., Cosme de Esteban, M., Espino, F., Haroun, R., et al. (2020). Testing side-scan sonar and multibeam echosounder to study black coral gardens: A case study from macaronesia. *Remote Sens.* 12, 3244. doi:10.3390/rs12193244
- de Matos, V., Gomes-Pereira, J. N., Tempera, F., Ribeiro, P. A., Braga-Henriques, A., and Porteiro, F. (2014). First record of antipathella subpinnata (anthozoa, antipatharia) in the azores (ne atlantic), with description of the first monotypic garden for this species. *Deep Sea Res. Part II Top. Stud. Oceanogr.* 99, 113–121. doi:10.1016/j.dsr2.2013.07.003
- Glogowski, S., Dullo, W.-C., Feldens, P., Liebetrau, V., von Reumont, J., Hühnerbach, V., et al. (2015). The eugen seibold coral mounds offshore Western Morocco: Oceanographic and bathymetric boundary conditions of a newly discovered cold-water coral province. *Geo-Marine Lett.* 35, 257–269. doi:10.1007/s00367-015-0405-7
- Goldberg, W. M., Hopkins, T. L., Holl, S. M., Schaefer, J., Kramer, K. J., Morgan, T. D., et al. (1994). Chemical composition of the sclerotized black coral skeleton (coelenterata: Antipatharia): A comparison of two species. *Comp. Biochem. Physiol. Part B Comp. Biochem.* 107, 633–643. doi:10.1016/0305-0491(94)90197-x
- Gray, J. E. (1857). Synopsis of the families and genera of axiferous zoophytes or barked corals. *Proceedings of the Zoological Society of London* 25 (1), 278–294. Available online at: <https://www.biodiversitylibrary.org/page/32451423>
- Hamana, M., and Komatsu, T. (2021). Mapping 3d structure of a sargassum forest with high-resolution sounding data obtained by multibeam echosounder. *ICES J. Mar. Sci.* 78, 1458–1469. doi:10.1093/icesjms/fsab044
- Heinrich, C., Feldens, P., and Schwarzer, K. (2017). Highly dynamic biological seabed alterations revealed by side scan sonar tracking of lanice conchilega beds offshore the island of sylt (German bight). *Geo-Marine Lett.* 37, 289–303. doi:10.1007/s00367-016-0477-z
- Held, P., and Schneider von Deimling, J. (2019). New feature classes for acoustic habitat mapping—A multibeam echosounder point cloud analysis for mapping submerged aquatic vegetation (sav). *Geosciences* 9, 235. doi:10.3390/geosciences9050235
- Lim, A., Wheeler, A. J., and Conti, L. (2020). Cold-water coral habitat mapping: Trends and developments in acquisition and processing methods. *Geosciences* 11, 9. doi:10.3390/geosciences11010009
- Lurton, X., Lamarche, G., Brown, C., Lucieer, V., Rice, G., Schimel, A., et al. (2015). Backscatter measurements by seafloor-mapping sonars: Guidelines and recommendations. A collective report by members of the GeoHab backscatter working group. Available at: <http://geohab.org/wp-content/uploads/2013/02/BWSG-REPORT-MAY2015.pdf>. 1–200.
- McGonigle, C., Grabowski, J. H., Brown, C. J., Weber, T. C., and Quinn, R. (2011). Detection of deep water benthic macroalgae using image-based classification techniques on multibeam backscatter at cashes ledge, gulf of Maine, USA. *Estuar. Coast. Shelf Sci.* 91, 87–101. doi:10.1016/j.ecss.2010.10.016
- Minami, K., Tojo, N., Yasuma, H., Ito, Y., Nobetsu, T., Fukui, S.-i., et al. (2014). Quantitative mapping of kelp forests (laminaria spp.) before and after harvest in coastal waters of the shiretoko peninsula, hokkaido, Japan. *Fish. Sci.* 80, 405–413. doi:10.1007/s12562-014-0731-0
- Parnum, I., and Gavrilov, A. (2012). High-frequency seafloor acoustic backscatter from coastal marine habitats of Australia. *Proc. fo Aust. Soc. Aust.* 5, 13–26. doi:10.3723/ut.30.013
- Pavlis, N. K., Holmes, S. A., Kenyon, S. C., and Factor, J. K. (2012). The development and evaluation of the Earth gravitational model 2008 (egm2008). *J. Geophys. Res. solid earth* 117, B04406. doi:10.1029/2011jb008916
- Porskamp, P., Schimel, A. C. G., Young, M., Rattray, A., Ladroit, Y., and Ierodiaconou, D. (2022). Integrating multibeam echosounder water-column data into benthic habitat mapping. *Limnol. Oceanogr.* 67, 1701–1713. doi:10.1002/lno.12160
- Roark, E. B., Guilderson, T. P., Dunbar, R. B., and Ingram, B. L. (2006). Radiocarbon-based ages and growth rates of Hawaiian deep-sea corals. *Mar. Ecol. Prog. Ser.* 327, 1–14. doi:10.3354/meps327001
- Roberts, J. M., Brown, C. J., Long, D., and Bates, C. R. (2005). Acoustic mapping using a multibeam echosounder reveals cold-water coral reefs and surrounding habitats. *Coral Reefs* 24, 654–669. doi:10.1007/s00338-005-0049-6
- Rossi, S., Bramanti, L., Gori, A., and Orejas, C. (2017). *Marine animal forests: The ecology of benthic biodiversity hotspots*. Cham: Springer.
- Rossi, P., Ponti, M., Righi, S., Castagnetti, C., Simonini, R., Mancini, F., et al. (2021). Needs and gaps in optical underwater technologies and methods for the investigation of marine animal forest 3d-structural complexity. *Front. Mar. Sci.* 8, 591292. doi:10.3389/fmars.2021.591292
- Schimel, A. C., Brown, C. J., and Ierodiaconou, D. (2020). Automated filtering of multibeam water-column data to detect relative abundance of giant kelp (macrocyctis pyrifera). *Remote Sens.* 12, 1371. doi:10.3390/rs12091371
- Schneider von Deimling, J., and Weinrebe, W. (2014). Beyond bathymetry: Water column imaging with multibeam echo sounder systems. *Hydrogr. Nachr.* 31, 6–10.
- Schneider von Deimling, J., Brockhoff, J., and Greinert, J. (2007). “Flare imaging with multibeam systems: Data processing for bubble detection at seeps,” in 2013 OCEANS - San. Diego 8, 6. doi:10.1029/2007GC001577
- Schulze, I., Wilken, D., Zettler, M. L., Gogina, M., Schönke, M., and Feldens, P. (2021). Laboratory measurements to image endobenthos and bioturbation with a high-frequency 3d seismic lander. *Geosciences* 11, 508. doi:10.3390/geosciences11120508
- Snellen, M., Simons, D. G., and Riethmueller, R. (2008). High frequency scattering measurements for mussel bed characterisation. *J. Acoust. Soc. Am.* 123, 3627. doi:10.1121/1.2934852
- Weinrebe, W. (2020). Observations of marine life in the indian ocean by hydroacoustic water column imaging. *Hydrogr. Nachr.* 117, 6–12. doi:10.23784/HN117-01
- Wyllie, K., Weber, T., and Armstrong, A. (2015). “A review of wreck least depths,” in U.S. Hydrographic Conference 2015, Washington, DC, Mar 19, 2015. THSOA.